Magnetic Resonance-Compatible Tactile Force Sensor Using Fiber Optics and Vision Sensor

Hui Xie, *Student Member, IEEE*, Allen Jiang, Helge A Wurdemann, Hongbin Liu, *Member, IEEE*, Lakmal D. Seneviratne, *Member, IEEE*, and Kaspar Althoefer, *Member, IEEE*

***Abstract*— This paper presents a fiber optic based tactile array sensor that can be employed in magnetic resonance environments. In contrast to conventional sensing approaches, such as resistive or capacitive-based sensing methods, which strongly rely on the generation and transmission of electronics signals, here electromagnetically isolated optical fibers were utilized to develop the tactile array sensor. The individual sensing elements of the proposed sensor detect normal forces; fusing the information from the individual elements allows the perception of the shape of probed objects. Applied forces deform a micro-flexure inside each sensor tactel, displacing a miniature mirror which, in turn, modulates the light intensity introduced by a transmitting fiber connected to a light source at its proximal end. For each tactel, the light intensity is read by a receiving fiber connected directly to a 2-D vision sensor. Computer software, such as MATLAB, is used to process the images received by the vision sensor. The calibration process was conducted by relating the applied forces to the number of activated pixels for each image received from a receiving fiber. The proposed approach allows the concurrent acquisition of data from multiple tactile sensor elements using a vision sensor such as a standard video camera. Test results of force responses and shape detection have proven the viability of this sensing concept.**

***Index Terms*— Tactile array sensor, fiber optics, vision sensor.**

I. Introduction

ROBOTICS research is becoming more intrusive and important in our daily lives. Many robot devices have been developed to imitate human behavior in order to collaborate with humans or conduct arduous and dangerous tasks such as industrial assembly line manufacturing [1] or dismantling bombs. With more advanced robotics technology being developed, new application areas are becoming a reality: new robot systems are introduced in the operating theatre and are capable of conducting minimally invasive surgery (MIS) [2]. The efficacy and reliability of surgical applications have been enhanced by advanced mechanisms design, control theory and sensing technology, which were initially intended for industrial use. Compared to humans, a surgical robot can provide higher precision and accuracy, combined with automatically carrying out repetitive motions allowing the surgeon to focus on the essential aspects of the surgical task. Furthermore, modern robotic surgery tools can be designed and fabricated at a small size thus enabling surgeons to carry out operations minimally invasively through much smaller incisions, when compared to traditional open surgery [3].

Minimally invasive surgery is a type of surgery where the operation is performed through small incisions employing specially designed medical tools such as laparoscopic instruments or miniature manipulators [4]. The instruments usually include a viewing instrument known as an endoscopic or laparoscopic camera. During the procedure, these tools are inserted through narrow openings allowing the surgeon to view the inside of the patient and to conduct operations such as suturing, ablation and generally, the manipulation of organs. Master-slave configuration robots like the da Vinci system [5] have revolutionized minimally invasive surgery over the past decade. Despite some controversy concerning the clear benefits of the da Vince system, a trend of robotics systems becoming more prevalent in the operating room is observable, mainly due to advantages such as reduced pain and blood loss in patients, decreased chances of infections, and shorter patient recovery periods as well as shorter learning curves for surgeons [2].

It is standard practice to pre-operatively plan the surgery based on computerized tomography (CT). CT scans taken before the operation provide the surgeon with a good view of the patient's anatomy and the target area. However, eliminating radiation exposure to patients and medics while providing much higher soft tissue details, Magnetic Resonance Imaging (MRI) has established itself as an alternative pre-operative imaging tool for operation planning. CT is also widely used during operations, directly guiding surgeons whilst conducting minimally invasive procedures. However, long-term exposure to the x-ray radiation limits the applicability of this method in this context. Due to the recent advances in the field of MRI scanner technology and associated MR image processing methods, MRI scanning has now real-time or near real-time capability and is suitable for intra-operative image guidance [7]. One of the main limitations of MRI scanners is that any tool to be used inside the scanner bore or in its close vicinity needs to be MR compatible [8], i.e. any instrument or device used near the scanner needs to avoid usage of magnetic material in order not to be affected by the MR signals and not to distort the images [9].

Manuscript received June 6, 2013; revised August 1, 2013 and September 6, 2013; accepted September 9, 2013. Date of publication September 6, 2013; date of current version January 17, 2014. This work was supported by the European Commission's Seventh Framework Programme under Project STIFF-FLOP under Grant 287728. This is an expanded paper from the IEEE SENSORS 2012 Conference. The associate editor coordinating the review of this paper and approving it for publication was Dr. William N. MacPherson.

The authors are with the Centre for Robotics Research, Department of Informatics, King's College London, London WC2R 2LS, U.K. (e-mail: hui.xie@kcl.ac.uk; allen.jiang@kcl.ac.uk; helge.wurdemann@kcl.ac.uk; hongbin.liu@kcl.ac.uk; lakmal.seneviratne@kcl.ac.uk; k.althoefer@kcl.ac.uk).

Color versions of one or more of the figures in this paper are available online at http://ieeexplore.ieee.org.

Digital Object Identifier 10.1109/JSEN.2013.2281591

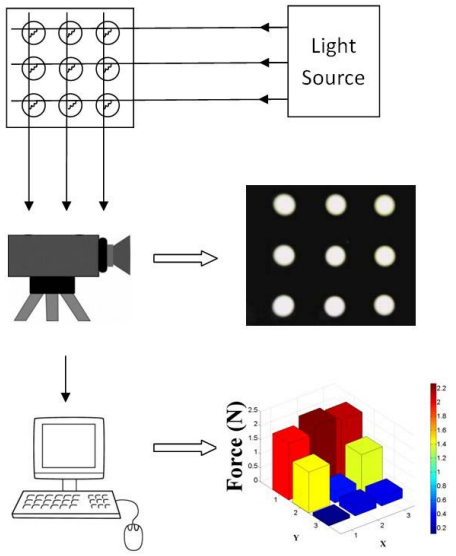

Fig. 1. Schematic of light intensity based tactile force sensor using camera.

Vision and imaging, in form of internally-applied laparoscopic cameras or external imaging techniques including CT and to a lesser extent MRI, have found wide-spread application in the modern operating theatre. However, the incorporation of other sensing modalities, such as force and tactile sensing, into medical devices and as a means to provide the surgeon with relevant information about the surgical site has been heavily neglected [10]. Signals from force and tactile sensors, especially in combination with visual information, are considered a powerful method to provide the surgeon with a better insight into and assessment of the geometrical and mechanical properties of the patient's organs such as shape, friction and stiffness.

Our work aims at creating a general-purpose tactile array sensor that can be employed in the MR environment to obtain organ properties that cannot be estimated using vision only. Acknowledging the potential of intra-operative MR imaging, we propose a force sensing paradigm that is based on fibre optics and the principles of light modulation, capable of augmenting images from MR scanners. This approach requires a complete design of the sensor system to ensure appropriate miniaturisation and MR compatibility. Commercial tactile and force sensors, such as the PPS TactArray and ATI Nano17, are not suitable because they are not magnetic resonance (MR) compatible.

This paper introduces a novel, fiber optic tactile sensing concept employing a 2D vision system for the acquisition of sensory information. The work is an expansion of our previous work [11]. We envisage for the actual sensing elements at the tip to contain an array of 3 $\times$ 3 force sensing tactels to be integrated with hand-held laparoscopic tools or remotely-operated surgical manipulators and to provide tactile information from the surface of probed organs, in particular soft-tissue organs. The schematic design of the presented sensor is then proposed and shown in Fig. 1. The project will address aspects relating to the design and fabrication of the array sensor and also investigate tactile sensor signal acquisition.

II. Methodology

A. Background

Research into tactile sensing reaches nearly as far back as research into vision, but has developed at a lower rate. The main reasons for this are that the tactile sensor needs to be in physical contact with the probed object all the time in order to perceive tactile information and, related to this, the acquisition of force and tactile sensor data is generally complex with numerous design requirements for the sensor, which needs to be capable of robustly acquiring sensor information during repeated physical interaction with objects [12].

There are a number of force sensing methods [13] that have been incorporated in tactile sensing systems. Current-based sensing [14] for example, which has a high accuracy, is one of the methods. However its power loss is also high compared to others. Resistive-based sensing [15] is based on the Ohm's Law, and the magnitude of the force is a function of the measured resistance value. One typical representative of this method is the strain gauge sensor [16], which measures force by translating the strain of the sensor structure caused by an applied force into electrical resistance. It has been widely used in many applications; however, it is sensitive to temperature variations. Although it is easy to manufacture at a small scale, its relatively low precision has limited its usefulness. Piezoelectric-based sensing [17] makes use of the piezoelectric effect (electricity generated by pressure) to measure force and acceleration. The feature of nearly zero deflection has brought it into wide-spread industrial use; however, it is not suitable for static measurements [18]. Capacitive-based sensing [19] is widely used these days due to its low cost, easy fabrication and insensitivity to temperature. The principle of this sensor is a capacitance change in accordance to either the distance between two capacitor plates or the amount of overlap between them. However, it suffers from sudden electrostatic discharge introducing noise and there is the likelihood that the discharge damages other electronic components in the vicinity. Magnetic-based sensors are based on magneto-elastic materials [20], which affect the magnetic transduction by the movement of a magnet or deformation of the core of a transformer or inductor caused by an applied force. It is physical robust with virtually no mechanical hysteresis [21]. Vision-based sensing [22] has caught many researchers' interest due to the availability of well-established computer vision systems and techniques [23]. Vision-based tactile sensing systems make use of small-sized cameras integrated with the tip of the probing tool and allows detecting force or stiffness via image processing [24], [25]. It could be widely used if its precision and response frequency were increased. It is noted that none of the above sensors can be deployed in a magnetic resonance scenario as they make use of non-MR compatible components located in the sensing area. Sensor containing metallic materials will be attracted by the powerful magnetic field thus the results may vary according to the environment and may even interfere with the MR imaging process itself - this requirement can be easily satisfied by the fiber optic sensor.

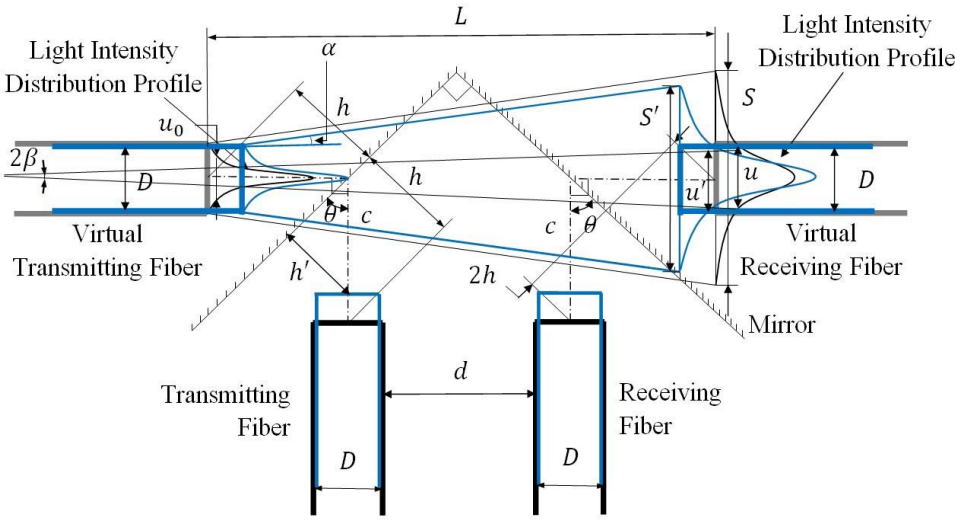

Fig. 2. Geometry of the light intensity modulation mechanism using prismatic mirror and a pair of parallel optical fiber.

Fiber optic-based sensing [26] is an area of great interest, as it allows the creation of small-sized and light-weight sensors, capable of operating in harsh environments. In addition, sensors based on this principle can be used in MR scanners. There are four main types of fiber optics sensing approaches currently employed where the modulation of the sensor signal is based on the wavelength, the phase, the polarization and the intensity, respectively. Fiber Bragg gratings (FBG) sensor [27] is the most commonly used wavelength modulated sensor, which reflects light of a particular wavelength depending on the placing of a periodic variation of the refractive index within a fiber core. It is sensitive to temperature and the associated measurement system may be expensive or complex. Using phase modulation, applied forces are determined interferometerically by comparing the phase of a signal fiber and reference fiber using an interferometer, such as those based on Mach-Zehnder and Fabry-Perot principles [28]. This approach is usually highly sensitive and accurate; however, sophisticated manufacturing is required to achieve the overall sensor system. The main types of polarization-based sensing [29] include linear, elliptical and circular polarization methods. The output signal is detected by the polarization state change due to stress or strain. Polarization modulated sensors are usually more expensive and difficult to use compared to the other sensor types. Intensity modulated sensors make use of the light intensity which is altered depending on the reflection, transmission or micro fiber bend affected by the magnitude of the causing variable, such as applied force. Its versatility, simple design, inexpensiveness and insensitiveness to temperature changes make it a strong contender for many applications. Because of these advantages and past experience in our research group with light intensity modulation sensors, we decided to make use of this principle for the sensor system described here.

B. Mathematical Model of Light Intensity Modulation

A geometrical representation of the light intensity modulation fiber optic based mechanism is shown in Fig. 2. Two fibers (a transmission fiber and a receiving fiber) distance d apart face a 90° double-mirror assembly at an angle of $\theta = 45°$ with regards to the mirror. Virtual transmission and receiving fibers are introduced to simplify the mathematical derivations; however, the light path between the virtual fibers is exactly the same as between the real fibers, assuming that the employed mirrors are perfectly reflecting transmitted light. All fibers have the same diameter, D.

The distance between the center of the fiber and the mirror is h. The virtual fibers are facing each other directly and their tips are distance L apart, i.e. the length of the light path between the tips of the real fibers is the same as the length of the light path between the virtual fibers

$$L = \frac{2h}{\sin\theta} + D + d. \tag{1}$$

The light transmitted to the receiving fiber (virtual and real) has a projection diameter S,

$$S = 2 \cdot L \cdot \tan\alpha + D = 2\tan\alpha \left(\frac{2h}{\sin\theta} + D + d\right) + D \tag{2}$$

where α is the radiation angle. S is the maximum projection diameter during force applied which would decrease the projection diameter explained in the following. When a force is applied, the mirror shifts downwards by distance x: this is equivalent to the transmitting and receiving fibers shifting upwards by the same distance of x, also shown in Fig. 2. Hence, the projection diameter is changing to

$$\begin{aligned} S' &= 2\tan\alpha \left(\frac{2h'}{\sin\theta} + D + d\right) + D \\ &= 2\tan\alpha \left[\frac{2(h - x \cdot \cos\theta)}{\sin\theta} + D + d\right] + D. \end{aligned} \tag{3}$$

The Gaussian form of the light intensity distribution model proposed in [30] is used for this sensor design, and modelled as follows:

$$I_{(r)} = I_o e^{\left(\frac{2r^2}{u_0^2}\right)} \tag{4}$$

where r is the light beam's radial distance, I_r is the intensity of the beam, $I_{(o)}$ is the beam's maximum intensity and u_o is the mode-field radius, the Gaussian width of the light transmitted out of the fiber, which is a constant parameter.

There is no boundary on the Gaussian curve and the light is theoretically distributed up to infinity, so it is assumed that the mode-field diameter is the boundary for calculation. Then the total light flux of the virtually transmitting fiber can be estimated as

$$\Phi_{VT} = \int_0^{\frac{S}{2}} I_{(r)} 2\pi r dr \approx \int_0^{\infty} I_o e^{\left(\frac{2r^2}{{u_0}^2}\right)} 2\pi r dr = \frac{I_o \pi {u_o}^2}{4} \quad (5)$$

where Φ_{VT} is the total virtually transmitted light flux. When distance s decreases, the light intensity I increases, however, the total light flux stays the same. The change of light intensity is in accordance with mode-field radius u_o. Defining ΔI_o and I_o' as the maximum intensity of the light projected at the tip of virtual transmitting fiber and the variation of maximum light intensity between virtual transmitting and receiving fibers, we obtain the following relations:

$$\Delta I_o = I_o' - I_o = \frac{4\Phi_{VT}}{\pi {u_o}^2} - \frac{4\Phi_{VT}}{\pi u^2} = \frac{4\Phi_{VT}}{\pi}\left(\frac{1}{{u_o}^2} - \frac{1}{u^2}\right) \quad (6)$$

where

$$u = \left[\frac{2(h - x \cdot \cos\theta)}{\sin\theta} + D + d\right]\tan\beta + u_o \quad (7)$$

and where β is the divergence angle. It is noted that the light flux transmitted to the receiving fiber is the light in the circular area with diameter d, which is the size of the receiving fiber, not the total light flux Φ_{VT}.

Then the maximum light flux collected by the receiving fiber can be calculated as

$$\Phi_r = \int_0^{\frac{d}{2}} I_{(r)} 2\pi r dr = \frac{I_o \pi u^2 \left(1 - e^{-\frac{D^2}{2u^2}}\right)}{2} \quad (8)$$

where Φ_r is the receiving fiber's maximum collected light flux as the minimum distance between optical fiber and reflective surface. Therefore, the light information "seen" at the site of the camera placed at the end of receiving fiber is

$$N = k\Phi_r = \frac{k I_o \pi u^2 \left(1 - e^{-\frac{D^2}{2u^2}}\right)}{2} \quad (9)$$

where N is the number of the activated pixels in the sensing area; hence, we call our approach pixel-based force sensing method. The normalized output can be represented as the ratio between the numerical value and its maximum value N_{max} as follows:

$$\frac{N}{N_{max}} = \frac{\frac{k I_o \pi u^2 \left(1 - e^{-\frac{D^2}{2u^2}}\right)}{2}}{max\left[\frac{k I_o \pi u^2 \left(1 - e^{-\frac{D^2}{2u^2}}\right)}{2}\right]}. \quad (10)$$

Two optical fibers (core diameter 1mm, reflective index 1.49 and numerical aperture 0.53) are placed parallel to each other and with a distance of 2mm between them - one for transmitting light from a 4 Watt LED torch and the other receiving light that is coupled into a Microsoft VX-800 camera. The 90° double-mirror attached to an ABS (acrylonitrile butadiene styrene) support is mounted on a linear motion platform. The test is conducted 3 times and the responses from the camera are recorded corresponding to the distance change between mirror and fiber at increments of 0.1mm from 0 to 1.7mm. A comparison of experimental data and simulated curve is shown in Fig. 3.

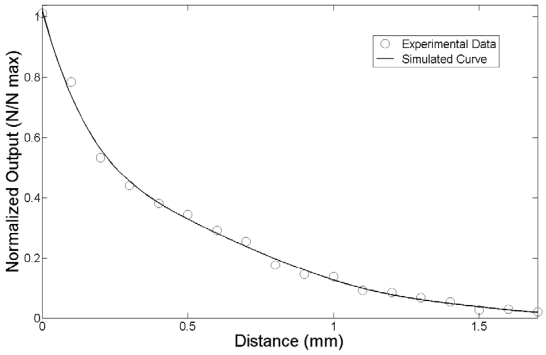

Fig. 3. Normalized experimental data and output from light intensity modulation model.

III. Sensor Design

At this stage, the authors have successfully used fiber optics to build a 3 by 3 tactile sensor based on the principle of light intensity modulation. Previous work on intensity modulated fiber optic sensors uses a pair of parallel optical fibers [31] with one projecting light into the other fiber via a reflecting surface. Once the distance between the fibers and the surface changed in response to external environment changes, the variation of the light intensity received will be detected to measure the related physical factor, such as force. Another similar approach is using the bent-tip optical fibers [32] to augment the performance by avoiding the loss of light during transmitting and receiving in the transduction procedure. Also, the use of a coupler to couple two individual fibers into one single fiber [33] is one of the popular ways to design a fiber optic sensor. In such a design, the light is transmitted and received in the same fiber thus more light can be collected compared to parallel displaced fiber optic sensors. The disadvantage of using a coupler is the high cost and manufacturing difficulties in displacing the fibers and connecting them.

The comparison of bent-tip optical fibers and parallel optical fibers has been presented by Puangmali [30], in which force is calibrated by voltage generated from the light intensity through an optoelectronic circuit. Puangmali et al. conclude that bent-tip optical fibers are more sensitive than parallel displaced optical fibers (in both cases, i.e. if laterally or longitudinally moving) and provide a wider working range. The study has also concluded that 90 degrees between the two bent-tip optical fibers is the more appropriate angle to detect small displacement changes – we have adopted this approach for the tactile sensor presented in this paper.

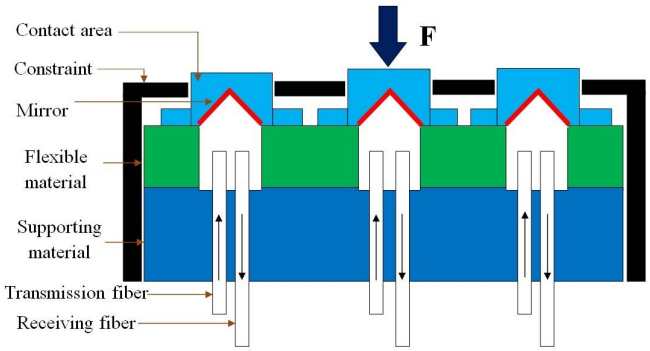

Fig. 4. Design of tactile sensor with mirror displacement.

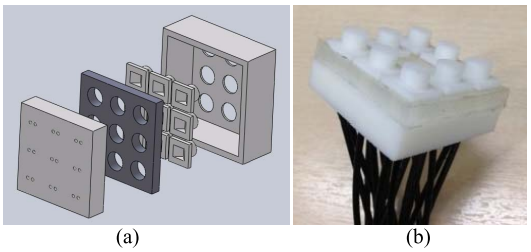

(a) (b)

Fig. 5. (a) CAD drawing of proposed sensor, (b) photo of proposed sensor tip.

The main structure of a fiber optic force sensor includes light source, transduction element and optical detector. Existing intensity modulation fiber optic sensors [34] are mostly based on a set of opto-electronics, where each opto-electronic receiver (consisting of a photodiode, photoresistor or phototransistor and a signal conditioning circuit) converts received light signals individually into voltage signals. It provides a sensitive response with low noise but is limited to low-resolution tactile arrays, because of high cost and complexity of detection elements and electronic circuits, if used in large numbers. To overcome this problem, a fiber optic sensor employing a 2D vision sensor (camera system) has been developed. Different from previously described vision-based sensors, the developed sensor uses a vision sensor to detect only the light intensity at the end of a receiving fiber rather than attaching it to the sensing tip. Thus, its simplicity, high resolution and low cost can be achieved in one go.

A. Sensor Hardware

The tactile sensor structure was designed in SolidWorks as shown schematically in Fig. 4 and printed by a rapid prototyping machine using ABS, Fig. 5. On top of the main, rigid structure of the sensor, silicone is used as the flexible element - the silicone layer behaves like a spring and its thickness decreases when a force is applied. A cylinder-like sensing element is developed as the contact area for the sensor to detect applied forces; inside the contact area two mirrors are placed at an angle of 45 degree to reflect light as introduced in the mathematical model section. As the sensor is designed to detect z-axis force information, any x and y movements which would affect the sensor performance should be avoided. In this case, the top layer was designed in such a way to constrain the x and y movement of the sensing elements.

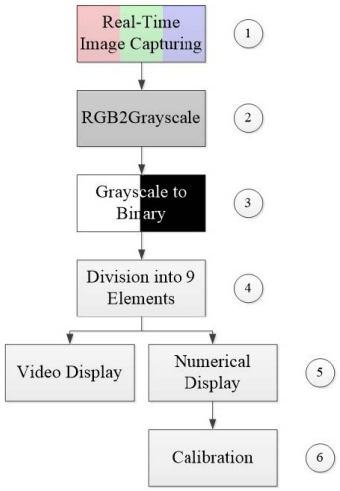

Fig. 6. Simulink Flowchart.

B. Sensor Software

The change of light intensity of each reflected fiber is used to determine the force applied to the sensor array. The methodology shown in Fig. 6 illustrates the sequence followed from capturing the real-time image to finally deriving the amount of force, and the sequence of image processing is shown in Fig. 7. The algorithm is implemented in a Simulink/Matlab model and can be summarized as follows:

1. Capturing the real-time video images.
2. The RGB image is transformed into a grayscale image. The following equation was used in the algorithm to convert the intensity image from the three layered RGB image enabling the detection of light changes:

$$I = 0.2989\ R + 0.5870\ G + 0.1140\ B \tag{11}$$

where I is the light intensity, R, G, and B represents red, green and blue value of each pixel.

3. The intensity image is then transferred to a binary image using a sufficient threshold which is calculated by the algorithm to eliminate the light noise from the outside environment:

$$n_i = \begin{cases} 0, & I_i < I_{threshold} \\ 1, & I_i > I_{threshold} \end{cases} \tag{12}$$

where n is the numerical value of each pixel, $I_{threshold}$ is the defined intensity threshold to eliminate ineffective pixels.

4. As the tactile array sensor contains different force information for specific areas of the sensor, the real-time video data is divided into 9 parts, each representing one sensing element.
5. Then the quantity of black and white pixels detected for each section is calculated:

$$N = \sum_{i=1}^{K} n_i \tag{13}$$

where N and K are the total numerical value and total number of the pixels in each sensing area.

6. Via a calibration algorithm, introduced in the following section, the force information applied on each sensing

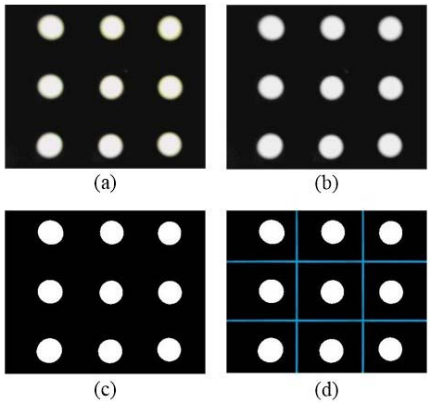

Fig. 7. Sequence of Image Processing: (a) Capturing images, (b) RGB2Grayscale conversion, (c) Binary image, (d) Division into 9 elements.

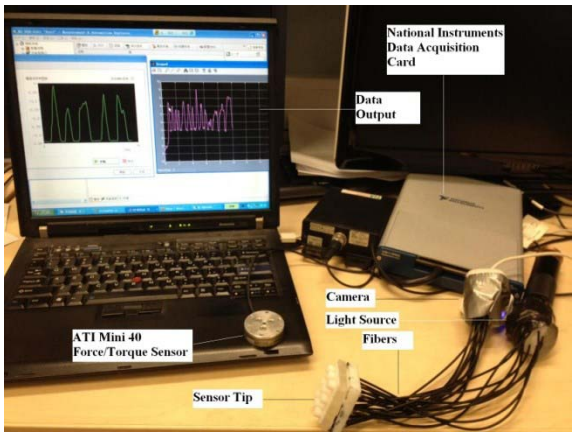

Fig. 8. Experimental set-up.

element is calculated as follows

$$f \propto N \tag{14}$$

where f is the applied force. The relationship between f and N is further investigated and demonstrated in the calibration process below.

IV. Test Setup and Results

A 4 Watt LED torch (Duracell Daylite) with light intensity of 160 lumens is used as the light source. A total of 18 optical fibers with the core diameter of 1mm are used. The core reflective index is 1.49 and the numerical aperture is 0.53. A high speed, low-cost USB camera (Microsoft VX-800) is installed to detect the light intensity changes, which are then transferred to a PC for further analysis. An ATI Mini 40 Force/Torque sensor attached to a National Instruments Data Acquisition Card is used to calibrate and test the static and dynamic response of the proposed sensor. The experimental set up is shown in Fig. 8.

A. Video Output

Once the sensing system has been switched on, the light information will be transferred from the light source to the unloaded sensing tip and then back to the camera. After the image processing (explained earlier), the binary light intensity images received from the nine sensor elements are displayed, as shown by the camera images of Fig. 9(a). Each of the white blobs represents the light intensity projected into the camera by one sensing element. Once a force is applied, the distance between mirror and transmission fiber and receiving fiber is decreased, resulting in an increase of the light intensity. Hence, the number of pixels in the camera image area corresponding to a sensing element will increase as an increased light intensity is received, as can be observed in the central blob of Fig. 9(b).

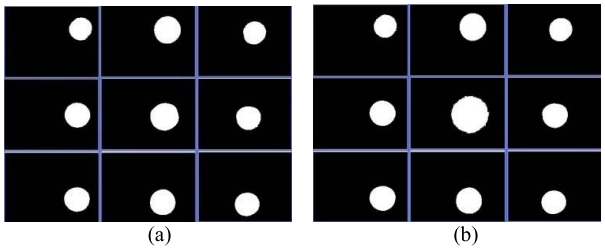

Fig. 9. (a) Unload status. (b) Force applied to sensing element that corresponds to the central element of the camera image.

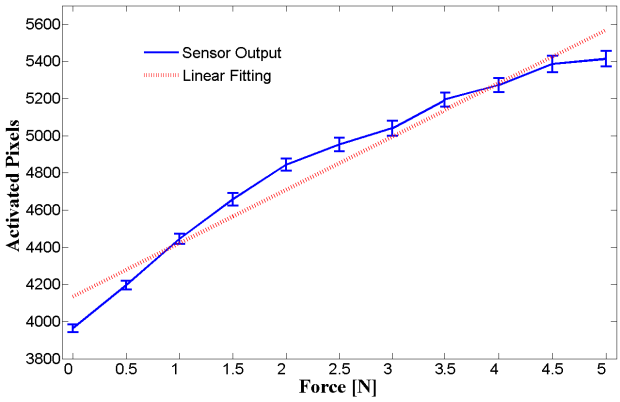

Fig. 10. Calibration data of element 5.

This approach lends itself to a straightforward way of visualizing applied forces. By analyzing the number of activated pixels using MATLAB, the relationship between the number of activated pixels and force applied can be used to calibrate the sensor.

B. Calibration

When forces are applied, the real-time data will be detected and recorded in Simulink. Fig. 10 shows the calibration results between applied force and average activated pixel numbers during 10 tests of one single element. Linear and quadratic fitting are also shown in the figure. The same calibration process is applied to all other sensing elements and the coefficients of the quadratic equation ($y = Ax^2 + Bx + C$, y is force, x is activated pixel number) and the linear fitting curve ($y = Dx + E$) are shown in Table I and Table II.

It can be seen from the Table I and II that the R-squared values of quadratic fitting for each sensing elements are higher

TABLE I
COEFFICIENT OF QUADRATIC FITTING CURVE

Sensor Number	Coefficients			
	A	B	C	R^2
1	7×10^{-5}	-0.2885	309.3	0.9895
2	2×10^{-5}	-0.1052	111.41	0.9944
3	2×10^{-4}	-0.6379	536.28	0.9796
4	4×10^{-5}	-0.2439	332.66	0.9934
5	2×10^{-6}	-0.0121	22.497	0.9971
6	1×10^{-5}	-0.0814	120.42	0.9943
7	1×10^{-5}	-0.0679	93.697	0.9808
8	5×10^{-5}	-0.3643	625.67	0.9956
9	-1×10^{-4}	0.6784	-1179.2	0.9410

TABLE II
COEFFICIENT OF LINEAR FITTING CURVE

Sensor Number	Coefficients		
	D	E	R'^2
1	0.0293	-66.83	0.9707
2	0.0229	-57.911	0.9884
3	0.0313	-52.773	0.9295
4	0.0292	-87.029	0.9856
5	0.0033	-13.683	0.9558
6	0.0081	-23.987	0.9347
7	0.0126	-39.138	0.9698
8	0.0236	-83.946	0.9873
9	0.026	-84.209	0.9323

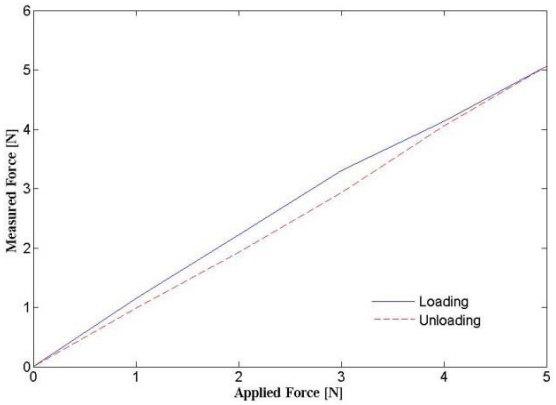

Fig. 11. Measured static response of a single element during loading and unloading. The hysteresis of the sensor is caused by the silicone.

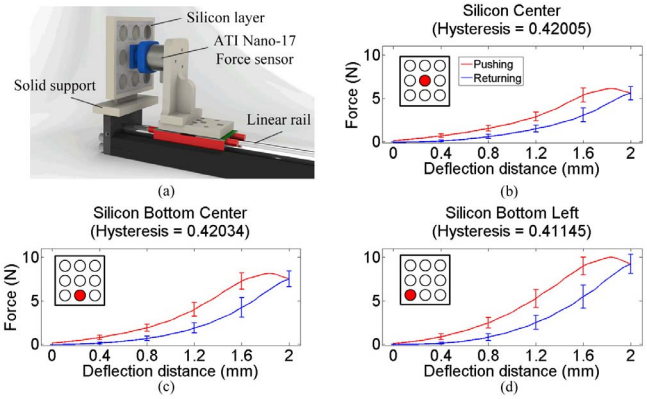

Fig. 12. Indentation hysteresis testing set-up (a), test results of the silicon layer for the center (b), bottom center (c), and bottom left corner (c).

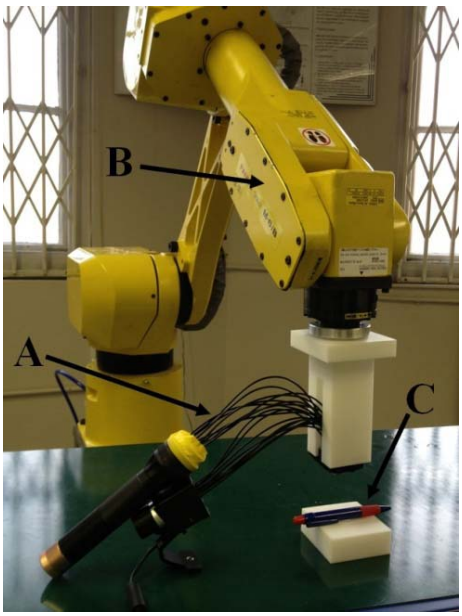

Fig. 13. Integration of optical fiber tactile sensor with robot arm (A: tactile force sensor, B: Robot manipulator, C: Testing platform).

than those obtained by linear fitting. However, as most of the R-squared values for linear fitting are close to 1 and the offsets from the actual sensor response and linear response caused by flexible material are within 0.5 N, the system has a reasonable linearity.

C. Static Response and Hysteresis Analysis

Using the ATI Mini 40 Force/Torque Sensor to test one element of the developed sensor after the calibration process, we obtain the data shown in Fig. 11. While some errors exist due to the hysteresis of the silicone material and noise that is introduced into our experimental system via the transmission and detection procedure, it still can be concluded that the pixel-based sensing principle is a way of detecting tactile information and developing high resolution tactile sensors. For the other 8 sensing elements, the same calibration equations with slightly different coefficients are established and further investigated in the following shape detection section.

To understand the repeatability and accuracy of the sensor, an analysis on the hysteresis effects on the silicon layer was performed, as shown in Fig. 12. Only the silicon layer was tested, as it is the sensors sole moving component. Three different areas of the silicon layer were tested: the center node, bottom center, and the bottom left corner. The test was performed by indenting the flexible material by 2 mm at a speed of 0.1 mm/second, followed by the reversed motion, returning the indenter to its original position. An ATI Nano17 force sensor attached to the indenter measured the force resulting from the indentation. Fig. 12 shows that the amount of hysteresis is 41–42%. It should be noted that the silicon continues to exert a force until the indenter has returned to the zero position, although the indenter is just touching the

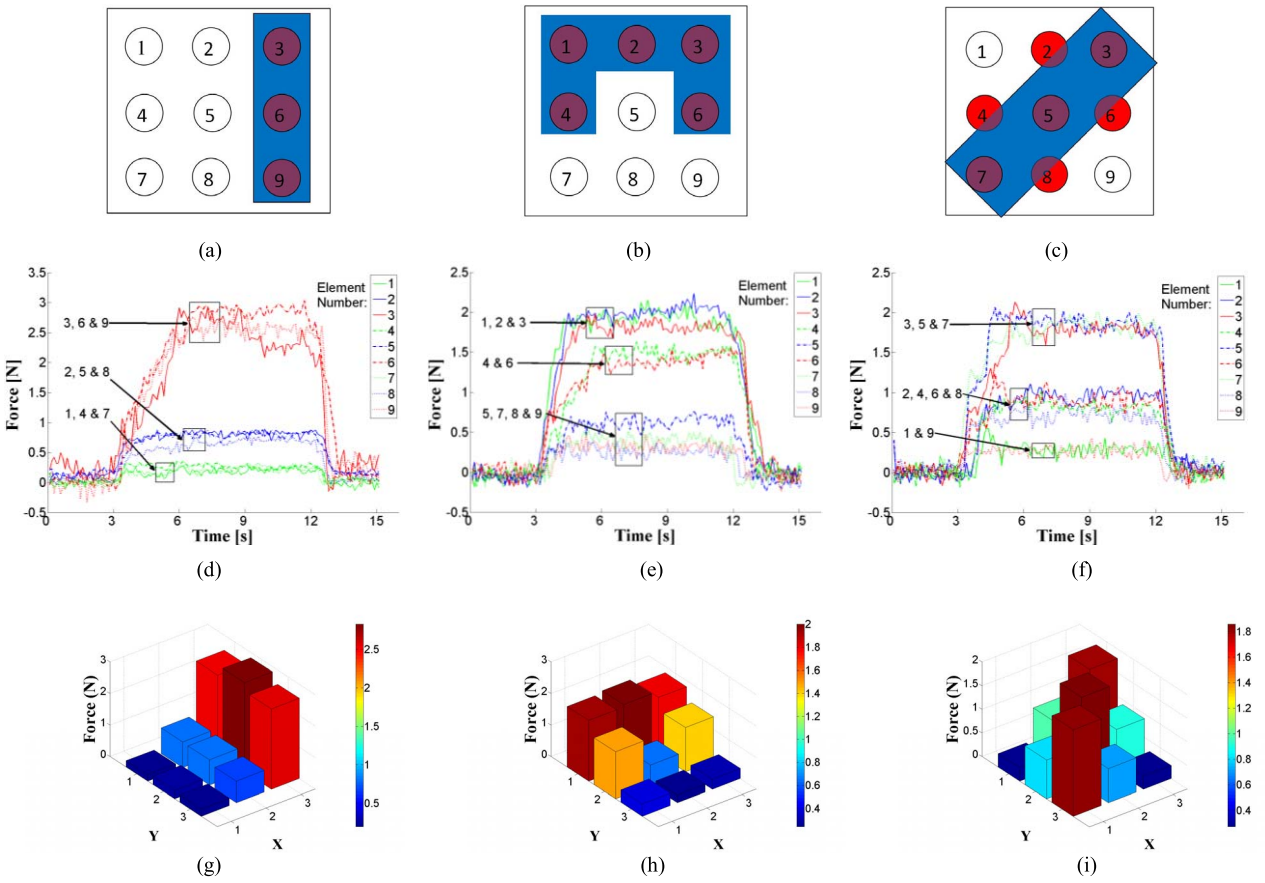

Fig. 14. Response of each individual sensing element during testing with different shapes and displacements (a), (d), (g) a rectangular-shaped object placed on the right side of the sensor, (b), (e), (h) a 'U'-shaped object placed on the top of the sensor, (c), (f), (i) a rectangular-shaped object diagonally placed in the middle of the sensor.

silicon. This indicates that the material is behaving elastically without permanent deformation. Thus, if indented and released at slower speeds, the amount of hysteresis would decrease. Additionally, the standard deviations for an indentation of up to 0.5 mm are 0.18, 0.20, and 0.25 N for the center, bottom center, and bottom left corner, respectively. At greater indentation distances, the standard deviations are larger indicating a lower accuracy at high indentations. Overall, the standard deviations are 0.34, 0.45, and 0.55 N for the center, bottom center, and bottom left corner, respectively. As can be seen from the results, even though the stiffness varies depending on the location of the sensor unit, the hysteresis changes only by a small amount (2%). The peak force measured for the center, bottom center, and left corner is 6.15, 8.16, and 9.99 N, respectively. Other than the hysteresis effect, sensor signal uncertainty is possibly also caused by other factors such as crosstalk between sensing elements, light signal loss especially in the connecting parts and mechanical misalignment between fibers. These aspects will be analyzed and alleviated as part of future research and development.

D. Shape Detection Test

To investigate the feasibility of the proposed array sensor, it was mounted on an industrial robot arm (FANUC M-6iB), as shown in Fig. 13. After the sensor was recalibrated using the standard force sensor (Section IV.B.), the robot arm is gradually moved down towards the testing platform until the output of the tactile sensor reaches 10 N. Differently shaped objects were attached to the platform and tested by the same procedure. The individual output of each sensing element during these test were recorded, Fig. 14.

During the test, the sensor started contacting the object at t = 3s and left the object at t = 12s, then the average output of each sensing element was calculated and displayed in a tactile image, Fig. 14(g), (h) and (i). For the first test, Fig. 14(a), forces applied on elements 3, 6 and 9 were successfully detected with a force value near 2.7 N. It is noted that the noise increases as the applied force increases on each sensing element. Also there exists a small crosstalk value, which the closer to the forces applied area, the bigger the value are (0.2 N–0.5 N). However, both are kept in an acceptable range thus not affecting the usefulness of the sensor in detecting contact area and force, which can also be seen from the following two tests, Fig. 14(b), (c). We believe that the crosstalk values between the fibers can even be used to further expand the resolution of the sensor [35]. Future work will address this point and also explore further sensor miniaturization.

V. Discussion and Conclusion

This paper presents the design of a laboratory prototype of a tactile array sensor using fiber optics and a 2D vision

sensor. Based on the light intensity modulation scheme, a camera system and Simulink interface were used to measure forces applied to each element of the array sensor acquiring tactile information. An additional advantage is that the sensing elements of the sensor are MR compatible and immune to electromagnetic noise. The proposed sensing structure and principle shows that the sensor can be miniaturized and achieve a high spatial resolution, and thus lends itself to integration with medical tools such as MIS instruments. The cost of the presented sensor is low compared to commercial tactile sensors, such as FBG-based sensors and Tekscan tactile sensors based on piezoresistive method

The proposed sensor will have many potential applications, not only in the manipulation of a humanoid robot, but also in bomb diffusion in a confined space, disaster response and rescue operations. However, our future work will focus on providing tactile sensing means for manipulation task as they may be conducted by humanoid robots and also to create highly miniaturized array sensors for robot-assisted minimally invasive surgery.

REFERENCES

[1] M. H. Korayem, N. Shiehbeiki, and T. Khanali, "Design, manufacturing, and experimental tests of a prismatic robot for assembly line," *Int. J. Adv. Manuf. Technol.*, vol. 29, nos. 3–4, pp. 379–388, 2006.

[2] B. Davies, "A review of robotics in surgery," *Proc. Inst. Mech. Eng. H, J. Eng. Med.*, vol. 214, no. 1, pp. 129–140, 2000.

[3] A. L. Trejos, J. Jayender, M. T. Perri, M. D. Naish, R. V. Patel, and R. Malthaner, "Robot-assisted tactile sensing for minimally invasive tumor localization," *Int. J. Robot. Res.*, vol. 28, no. 9, pp. 1118–1133, 2009.

[4] P. Puangmali, K. Althoefer, L. D. Seneviratne, D. Murphy, and P. Dasgupta, "State-of-the-art in force and tactile sensing for minimally invasive surgery," *IEEE Sensors J.*, vol. 8, no. 4, pp. 371–381, Apr. 2008.

[5] H. Tamás, J. Sándor, and Z. Benyó, "Surgery in space: The future of robotic telesurgery," *Surgical Endosc.*, vol. 25, no. 3, pp. 681–690, 2011.

[6] T. M. Peters, "Image-guided surgery: From X-rays to virtual reality," *Comput. Methods Biomech. Biomed. Eng.*, vol. 4, no. 1, pp. 27–57, 2001.

[7] G. Gang, S. Tarte, A. King, Y. Ma, P. Chinchapatnam, T. Schaeffter, R. Razavi, D. Hawkes, D. Hill, and K. Rhode, "Validation of the use of photogrammetry to register pre-procedure MR images to intra-procedure patient position for image-guided cardiac catheterization procedures," *Proc. SPIE*, vol. 6918, p. 69181Q, Mar. 2008.

[8] J. F. Schenck, "The role of magnetic susceptibility in magnetic resonance imaging: MRI magnetic compatibility of the first and second kinds," *Med. Phys.*, vol. 23, no. 6, pp. 815–850, Jun. 1996.

[9] P. Polygerinos, D. Zbyszewski, T. Schaeffter, R. Razavi, L. D. Seneviratne, and K. Althoefer, "MRI-compatible fiber-optic force sensors for catheterization procedures," *IEEE Sensors J.*, vol. 10, no. 10, pp. 1598–1608, Oct. 2010.

[10] M. H. Lee, "Tactile sensing: New directions, new challenges," *Int. J. Robot. Res.*, vol. 19, no. 7, pp. 636–643, 2000.

[11] H. Xie, A. Jiang, L. D. Seneviratne, and K. Althoefer, "Pixel-based optical fiber tactile force sensor for robot manipulation," in *Proc. IEEE Sensors*, Taiwan, Oct. 2012, pp. 1–4.

[12] H. Liu, J. Li, X. Song, L. D. Seneviratne, and K. Althoefer, "Rolling indentation probe for tissue abnormality identification during minimally invasive surgery," *IEEE Trans. Robot.*, vol. 27, no. 3, pp. 450–460, Jun. 2011.

[13] H. R. Nicholls and M. H. Lee, "A survey of robot tactile sensing technology," *Int. J. Robot. Res.*, vol. 8, no. 3, pp. 3–30, 1989.

[14] G. Tholey, A. Pillarisetti, W. Green, and J. P. Desai, "Design, development, and testing of an automated laparoscopic grasper with 3-D force measurement capability," in *Proc. Int. Symp. Med. Simul.*, pp. 38–48, 2004.

[15] F. Yi, A. L. Cabezas, Q. Chen, L. Zheng, and Z. Zhang, "Flexible UHF resistive humidity sensors based on carbon nanotubes," *IEEE Sensors J.*, vol. 12, no. 9, pp. 2844–2850, Sep. 2012.

[16] R. J. Stephen, K. Rajanna, V. Dhar, KG. K. Kumar, and S. Nagabushanam, "Thin-film strain gauge sensors for ion thrust measurement," *IEEE Sensors J.*, vol. 4, no. 3, pp. 373–377, Jun. 2004.

[17] J. Dargahi, "A piezoelectric tactile sensor with three sensing elements for robotic, endoscopic and prosthetic applications," *Sens. Actuators A, Phys.*, vol. 80, no. 1, pp. 23–30, 2000.

[18] C. Horst, T. Saito, and L. Smith, *Springer Handbook of Materials Measurement Methods*, vol. 978. New York, NY, USA: Springer-Verlag, 2006.

[19] C.-T. Ko, S.-H. Tseng, and M. S.-C. Lu, "A CMOS micro machined capacitive tactile sensor with high-frequency output," *IEEE/ASME J. Microelecromech. Syst.*, vol. 15, no. 6, pp. 1708–1714, Dec. 2006.

[20] A. B. Amor, T. Budde, and H. H. Gatzen, "A magnoelastic microtransformer-based microstrain gauge," *Sens. Actuators A, Phys.*, vol. 129, nos. 1–2, pp. 41–44, 2006.

[21] R. L. Shell and E. L. Hall, *Handbook of Industrial Automation*. Boca Raton, FL, USA: CRC Press, 2000, pp. 381–382.

[22] K. Kamiyama, H. Kajimoto, N. Kawakami, and S. Tachi, "Evaluation of a vision-based tactile sensor," in *Proc. IEEE Int. Conf. Robot. Autom.*, Apr./May 2004, pp. 1542–1547.

[23] O. Duran, K. Althoefer, and L. D. Seneviratne, "Automated sewer pipe inspection through image processing," in *Proc. IEEE ICRA*, vol. 3. May 2002, pp. 2551–2556.

[24] H. Dimitris, N. Ferrier, and R. W. Brockett, "The performance of a deformable-membrane tactile sensor: Basic results on geometrically-defined tasks," in *Proc. IEEE ICRA*, vol. 1. Apr. 2000, pp. 508–513.

[25] I. Yuji, Y. Kim, and G. Obinata, "Robust slippage degree estimation based on reference update of vision-based tactile sensor," *IEEE Sensors J.*, vol. 11, no. 9, pp. 2037–2047, Sep. 2011.

[26] K. T. V. Grattan and T. Sun, "Fiber optic sensor technology: An overview," *Sens. Actuators A, Phys.*, vol. 82, no. 1, pp. 40–61, 2000.

[27] S. J. Mihailov, "Fiber bragg grating sensors for harsh environments," *Sensors*, vol. 12, no. 2, pp. 1898–1918, 2012.

[28] Y. Toshihiko, K. Kurosawa, K. Itoh, and T. Ose, "Fiber-optic Fabry-Perot interferometer and its sensor applications," *IEEE Trans. Microw. Theory Tech.*, vol. 30, no. 10, pp. 1612–1621, Oct. 1982.

[29] S. Ramon, L. D. Seneviratne, and K. Althoefer, "A 2-axis optical force–torque fingertip sensor for dexterous grasping using linear polarizers," *IEEE Trans. Instrum. Meas.*, vol. 61, no. 12, pp. 1–15, Dec. 2012.

[30] P. Puangmali, K. Althoefer, and L. D. Seneviratne, "Mathematical modeling of intensity-modulated bent-tip optical fiber displacement sensors," *IEEE Trans. Instrum. Meas.*, vol. 59, no. 2, pp. 283–291, Feb. 2010.

[31] P. D. Goodyear, C. Fothergill, B. Jones, and D. Hanning, "The design of an optical fiber pressure transducer for use in the upper airways," *IEEE Trans. Biomed. Eng.*, vol. 43, no. 6, pp. 600–606, Jun. 1996.

[32] H. Liu, P. Puangmali, K. Althoefer, and L. D. Seneviratne, "Experimental study of soft tissue recovery using optical fiber probe," in *Proc. IEEE/RSJ Int. Conf. Intell. Robot. Syst.*, San Diego, CA, USA, Oct./Nov. 2007, pp. 516–521.

[33] P. Polygerinos, P. Puangmali, T. Schaeffter, R. Razavi, L. D. Seneviratne, and K. Althoefer, "Novel miniature MRI-compatible fiber-optic force sensor for cardiac catheterization procedures," in *Proc. IEEE ICRA*, May 2010, pp. 2598–2603.

[34] Y. Fu, H. Di, and R. Liu, "Light intensity modulation fiber-optic sensor for curvature measurement," *Opt. Laser Technol.*, vol. 42, no. 4, pp. 594–599, 2010.

[35] H. Liu, J. Greco, X. Song, J. Bimbo, L. D. Seneviratne, and K. Althoefer, "Tactile image based contact shape recognition using neural network," in *Proc. IEEE Conf. Multisensor Fusion Integr. Intell. Syst.*, Sep. 2012, pp. 138–143.

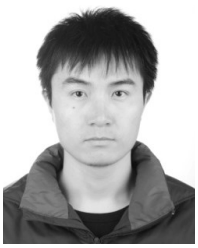

Hui Xie received the B.S. degree in automatic control from Northwestern Polytechnical University, Xi'an, China, in 2010. He then received the King's-China Scholarship Council and is currently pursuing the Ph.D. degree in tactile force sensors at the Center for Robotics Research, Department of Informatics, King's College London, London, U.K. His research interests include fiber optics, tactile sensing system, and image processing.

Allen Jiang received the B.S. degree in aerospace engineering from the University of California, San Diego, La Jolla, CA, USA, in 2010. He is currently pursuing the Ph.D. degree in flexible manipulators for medical applications at the Center for Robotics Research, Department of Informatics, King's College London, London, U.K. His research interests include granular jamming and robotics.

Helge A Wurdemann is a Research Associate with the Center for Robotics Research. He received the Dipl.-Ing. degree in electrical engineering from the Leibniz University of Hanover, Hanover, Germany. In 2006, he studied at the Auckland University of Technology, Auckland, New Zealand and carried out a research project with Loughborough University, Loughborough, U.K., in 2007. With funding from the EPSRC he conducted his Ph.D. studies and received the Ph.D. degree from King's College London in 2011. In November 2011, he was with the Research Team of Prof. K. Althoefer. His research interests include medical robotics for minimally invasive surgery.

Hongbin Liu is currently a Lecturer (Assistant Professor) with the Department of Informatics, King's College London (KCL), London, U.K. He received the B.S. degree from Northwestern Polytechnique University, Xi'an, China, in 2005, and the M.Sc. and Ph.D. degrees from KCL in 2006 and 2010. His research interests include the tactile/force perception based robotic cognition, the modeling of dynamic interaction, and medical robotics and haptics.

Lakmal D. Seneviratne (M'03) received the B.Sc.(Eng.) and Ph.D. degrees in mechanical engineering from King's College London (KCL), London, U.K., in 1980 and 1985, respectively. He is currently a Professor of robotics with Khalifa University, Abu Dhabi, U.A.E., on secondment from KCL, where he is a Professor of mechatronics. He has published over 250 refereed research papers related to robotics and mechatronics. His research interests include robotics and intelligent autonomous systems. He is a fellow of the Institution of Engineering and Technology and the Institution of Mechanical Engineers.

Kaspar Althoefer (M'03) received the Dipl.-Ing. degree in electronic engineering from the University of Aachen, Aachen, Germany, and the Ph.D. degree in electronic engineering from King's College London (KCL), London, U.K. He is currently a Professor of robotics and intelligent systems and the Head of the Center for Robotics Research, Department of Informatics, KCL. He has been involved in Research on mechatronics since 1992 and gained considerable expertise in the areas of sensing, sensor signal analysis, embedded intelligence, and sensor data interpretation using neural networks and fuzzy logic, as well as robot-based applications. He has authored or co-authored more than 180 refereed research papers related to mechatronics and robotics.